Journal of Visualization, Vol. 3, No. 1 (2000) 9-26

Particulars of the Cross- and Spanwise Near-wake Development of a Short Semicircular-section Shell, through the Transition *Re*-range ($60 \leq Re \leq 600$)

Coutanceau, M.*, Migeon, C.* and Ehrmann, P.*

* University of Poitiers - Laboratoire d'Etudes Aérodynamiques - UMR CNRS 6609, 86960 Futuroscope cedex - France.
e-mail : madeleine.coutanceau@univ-poitiers.fr

Received 1 April 1999.
Revised 22 October 1999.

***Abstract*:** Within the fundamental context of quasi-2D bluff-body near-wake investigation, we analyse the way the initial wake vortices (primary and secondary vortices) form and develop with time behind a short (5.2:1) cylindrical semicircular shell (hollow at the back), after an impulsive start in translation. The study includes the transition regime and non-usual cross-sectional shapes. The structure of the vortices is examined by means of precise visualizations both in the mid-cross and mid-span planes. The particulars induced by the hollow face are deduced from a comparison with the cases of analogous solid cylinders and more particularly with the full semicircular cylinder (Boisaubert et al., 1996; Coutanceau et al., 1998).

The crosswise analysis shows that, except some fundamental difference at the separation initiation and some differences in details, a similar development of the Bénard-Kàrmàn-vortices is observed, thus :

- the regime of the occurring structures changes beyond the first phase of development (i.e. $t^* \geq 6$) when Reynolds number is passing through a critical value Re_c (here $120 \leq Re_c \leq 140$)
- Kelvin-Helmholtz instabilities are detected for $Re = 600$ in the rolled-up separated shear layers originating from the sharp body-edges.

On the contrary, the spanwise analysis reveals that the hollow face plays an important role in the time-development of the induced body-end three-dimensionalities (end-vortices and opposite spanwise currents) and intrinsic three-dimensionalities respectively. Thus, as opposed to solid bodies similarly limited in span, the emergence of clear patterns of secondary Taylor-Görtler-like vortices in the near wake have been experimentally proved for the first time when *Re* passes beyond the transition value of $Re_t \approx 200$. The consequence on the global structure of the flow is deduced.

***Keywords*:** three-dimensional formation, cylindrical shell, cross and spanwise visualization, primary and secondary instabilities.

1. Introduction

During the past decade, the significant progress in understanding nominally two-dimensional bluff-body wakes should be noted. This is mainly the result of the sustained effort done by investigators to take into account the three-dimensional (3-D) degeneration of the flow structure, occurring inevitably in any flow placed in a realistic situation. In particular, a lot of very interesting investigations have been conducted to study the laminar-to-turbulent transition. However, some questions still remain without definitive answers. Initially, the questions arose from the physical origin of irregularities found in the vortex-shedding process and consequently in the Strouhal-Reynolds number relationship ($St(Re)$), first pointed out in the case of the long circular cylinder by Tritton

(1959) for $Re \approx 90$ (laminar regime) and by Rosko (1954) for $150 < Re < 300$ (transition regime). Since then, many points have been specified, including the critical values of the Reynolds number at which the discontinuities occur and successive explanations have been proposed; some of them are still under discussion. However, it is now clear that all are linked with the emergence of induced and/or intrinsic three-dimentionalities in the initially 2-D wake flow.

A detailed review on this subject has recently been published by Williamson (1996 a, b). It appears that the substantial step in understanding these wake-flows arose from matching the new experimental, numerical and analytical findings. Thus, from the experimental point of view, we note the emergence of more and more sophisticated techniques susceptible to provide new data, such as vorticity (Mansy et al., 1994; Wu et al., 1996; Chyu and Rockwell, 1996). On the other hand, very efficient 2-D, but also 3-D direct numerical simulations (Karniadakis and Triantafyllou, 1992; Tomboulides, Triantafyllou and Karniadakis, 1992; Zhang, Noack and Eckelmann, 1994; Zhang et al., 1995) have been elaborated as well as very interesting analytical approaches like those based on approximate or full Floquet stability analysis (Noack, König and Eckelmann, 1993; Noack and Eckelmann, 1994; Barkley and Henderson, 1996) or Ginzburg-Landau model (Albarède and Provansal, 1995, Leweke and Provansal, 1995, etc.). Each of them provided complementary insights. However, it appears that the origin and consequence of the detected three-dimensionalities are still debated and some data are still missing, even for the most popular case of a long circular-section cylinder. Furthermore, the respective influence of both the body length limitation and the cross-sectional shape is not really known, although, these data would be of primary importance in industrial applications. In the same way, it is not clear how these three-dimensionalities arise and settle with time after the start of the motion. At last, it is regularly regretted that not enough experiments have been devoted to the very sensitive wake-transition regime, especially by means of visualizations susceptible to show "in clear" the phenomena.

Here, using such visualization support, we consider the early wake-vortex formation behind a rather short (limited by two large endplates) cylindrical semicircular shell, the hollow face being at the back, after it has been subjected to an impulsive start from rest. This particular shape has been selected for both its practical and fundamental interest. Indeed, it may constitute a schematization of devices, or part of devices, encountered in industrial technology (antennas, burners, electrodes, wind-engine rotors, etc.). On the other hand, its concave downstream face generates a wake-flow particularly interesting to study the development of intrinsic three-dimentionalities with increasing Re. We show here that these instabilities provoke the emergence of well-formed Taylor-Görtler-type vortices when Reynolds number (Re) passes beyond a transition value ($Re_t \approx 200$). This is confirmed in Fig. 1(b). Figure 1 shows, in parallel, the primary (Fig. 1(a)) and secondary (Fig. 1(b)) wake instabilities: the flow patterns have been captured at the same time-stage of the wake development, for $Re = 400$, in the mid-cross (Fig. 1(a)) and mid-span plane (Fig. 1(b)). In Fig. 1(a) the flow runs from left to right, in Fig. 1(b) it runs upwards. The trace of the shell is viewed as a single white arc (Fig. 1(a)) and white straight line (Fig. 1(b)) respectively. The lower parts of the vertical traces of the endplates are visible in Fig. 1(b). A more complete description of the spanwise view will be given in Sec. 4.

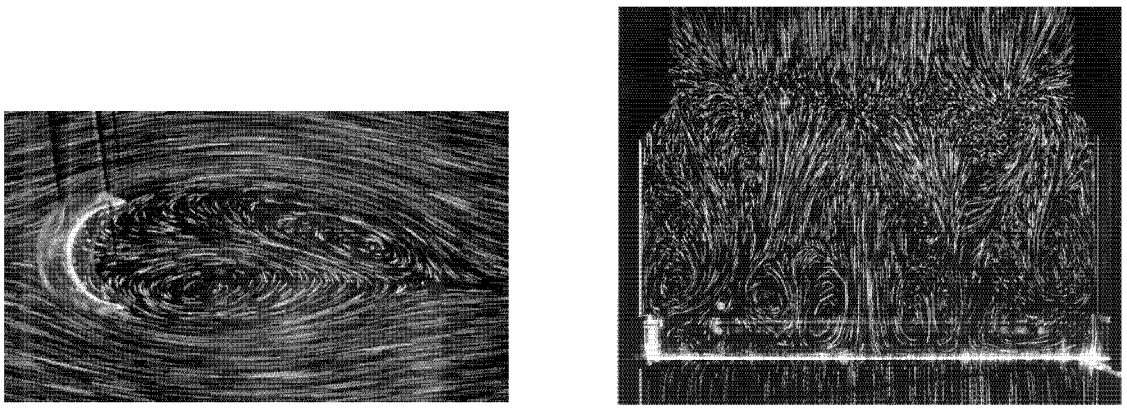

(a) (b)

Fig. 1. Example of flow structure in the mid-cross plane (a) and in the mid-span plane (b) downstream an abruptly started (5.2 in aspect ratio) cylindrical semicircular shell, limited by two endplates, at $t^* = 8$ and $Re = 400$; at the top, the incident flow is from left to right whereas, at the bottom, it runs upwards. On each picture, the upstream trace of the body trace is the thickest white line: arc (in (a)) or straight horizontal line (in (b)).

The shell body case was formerly examined by Taneda (1979), Hasimoto (1979), Abed-Meraïm and Coutanceau (1990), Abed-Meraïm (1992) for very low Reynolds numbers and by Massons et al. (1988) for very high Reynolds numbers.

The present study is based upon a detailed analysis of particle-streak and electrochemical-filament flow-visualization pictures (Coutanceau and Pineau, 1997). The pictures have been taken not only in the mid-cross plane but also spanwise to appreciate the 3-D degeneration of the flow structure. Except for this aspect, the experimental conditions and method of approach are the same as described by Boisaubert et al. (1996) to study the solid semicircular cylinder.

2. Method of Approach

The shell is towed in the vertical liquid-tank (460×560×1500 mm³) described by Boisaubert et al. (1996) and Coutanceau and Pineau (1997). Using the same starting-flow visualization techniques, the time-development of the flow around the shell can be observed in detail all along its uniform translation in the tank, as soon as it is impulsively started. The way the body is attached by means of two guiding rods hold to each endplate and the measurement of the different elements are given in Fig. 2. A sequential recording of the flow is automatically operated by a camera which accompanies the body in its motion, so that the body appears to be at rest and placed in a uniform incident stream V_0. The shell is made of half a (2 mm in thickness) plexiglas tube whose edges have been carefully chamfered. The diameter D of 80 mm is sufficiently large to assure precise visualization; the length of 416 mm implies an aspect ratio of 5.20. The successive values of the Reynolds number ($Re = V_0D/\nu$) effectively considered are 60, 100, 200, 400 and 600. For each of them, the flow was recorded during a period of normalized time $t^* = tV_0/D$ ranging from 0 (start of the motion) to 10, with a time step Δt^* of 0.5 or 1. Thus, the last flow recording is made after the body has travelled a distance equal to $10D$. For the explanation of such a time limit, see Boisaubert et al. (1996). A paraffin oil, having a suitable viscosity ($\nu = 1.52\ 10^{-5}$ m²/s) for the studied Re-range, has been selected for the particle-streak visualization, whereas it was necessary to use water for the generation of the electrochemical (tin salt) tracer. Consequently, only the greatest value of $Re = 600$ has been studied with the second method.

The same quantitative data, as those previously given by Boisaubert et al. (1996), have been extracted from the particle-streak pictures, such as the geometrical parameters of the forming recirculating zone, and the V_x-component of the velocity along the downstream ***x***-centeraxis (cf. Ehrmann, 1996). In the present paper, only the length L_{RZ} of the recirculation zone, as a function of Re and t^*, is given. However, other typical velocity profiles along an axis crossing the primary vortex in formation are added in order to estimate the degree of instability of the corresponding rotating flow.

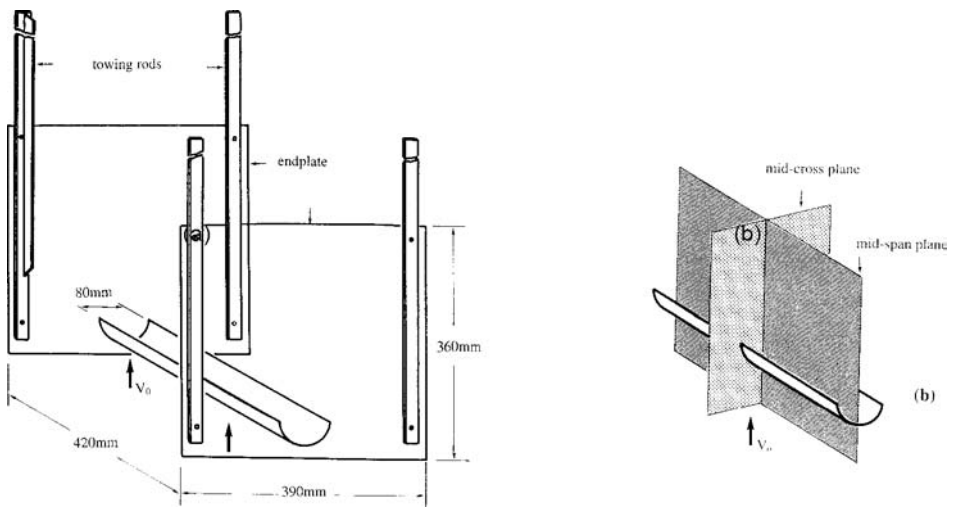

Fig. 2. Schematic of the experimental body arrangement (a) and light sheet disposition (b).

3. Wake-flow Structure in the Mid-cross Plane

At first, let us consider the time-evolution of the wake-flow structure visualized in the mid-cross plane.

An illustration of the general process related to the vorticity convection is given by the sequence of pictures of Fig. 3 for Re = 600 and $0.5 \leq t^* \leq 8.0$. They have been taken with the technique of the tin salt filament emitted from the body wall, exactly in the same manner as described by Ehrmann (1996) and Boisaubert et al. (1996). We see, very precisely, how the boundary layer separates from the body wall and rolls up into rapidly growing vortices. With increasing time, these vortices grow essentially in strength and in length, at first symmetrically, and then with a progressive increasing asymmetry. For this Re-value, the early occurrence of Kelvin-Helmholtz (K-H) instabilities should be noted. They are initially visible at the downstream part of the rolling-up (t^* = 3-4) and

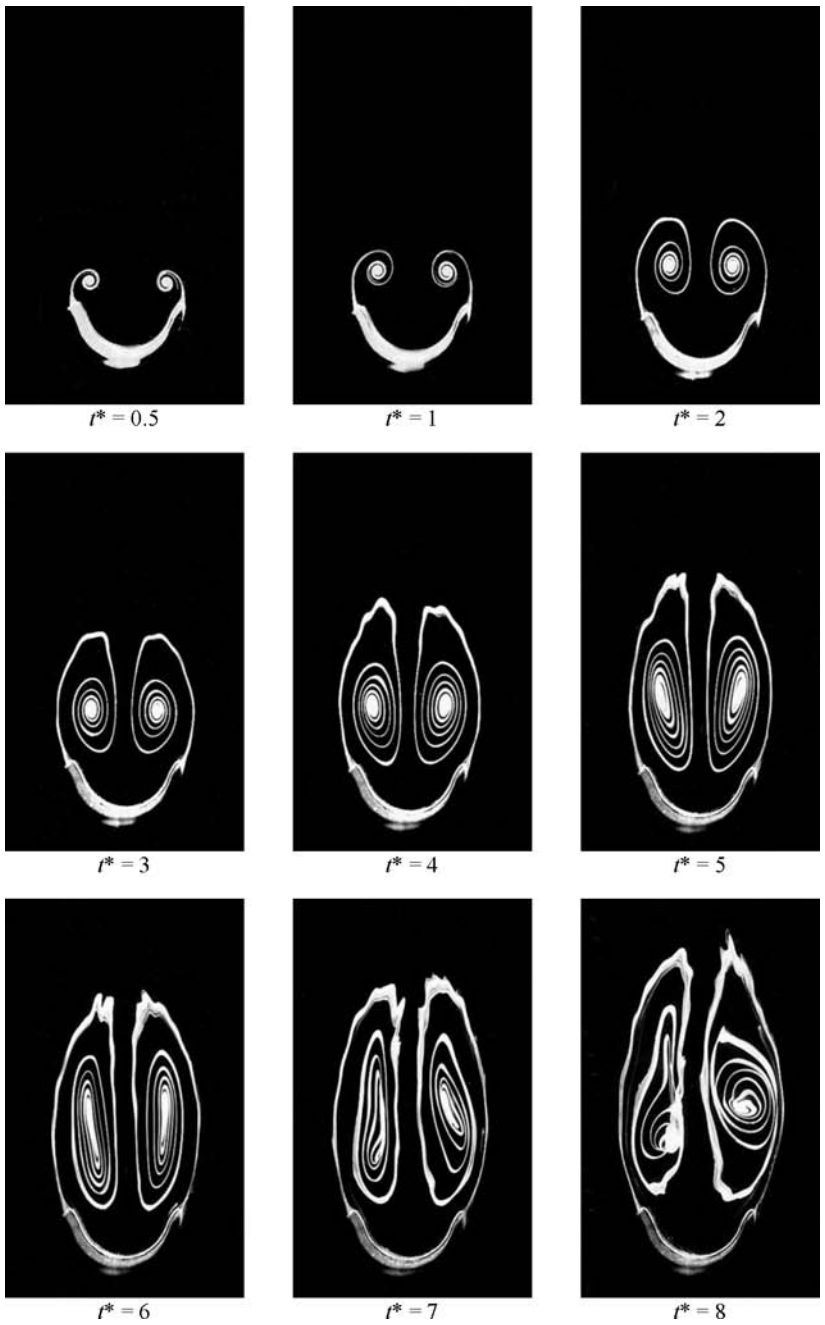

Fig. 3. Time sequence of the separated shear layer rolling-up behind a semicircular shell visualized by electrochemical filament emitted from the body wall for Re = 600; mid-cross-sectional view with the incident flow upwards.

progressively all along the filaments showing the progressive three-dimensional distortion of the vortex-cores. It is known that these K-H instabilities are promoted by the presence of the sharp edges of the body (Polidori et al., 1992; Polidori, 1994) and the increase of *Re*. In the case of the circular cylinder, they have been found to birth mostly for $Re \approx 1000$ (see Chyu and Rockwell, 1996). However, very recently, Prasad and Williamson (1997) showed that their first appearance (Re = 1200 or 2600) depends on the spanwise end-conditions and consequently on the primary mode of vortex shedding.

The electrochemical visualization is a very sensitive method to give evidence of the separated shear-layer instabilities. Unfortunately, this method could not been applied (without decreasing the body diameter and consequently the visualization definition) for $Re < 600$, because the corresponding experiments had to be carried out in oil (not suitable for the electrochemical process), as it was mentioned above. So most of the present data have been provided by means of the particle-streak method visualizing the velocity field like in the sequence of Fig. 4. The pictures present selected typical phases of the time wake-vortex evolution for Re = 100, from t^* = 1 up to t^* = 10 (limit of our experimental possibility, cf. Ehrmann, 1996). At this final time, three vortices had time to be or on the way to be shed. A stricking resemblance with the corresponding pictures of the solid semicircular cylinder case (cf. Boisaubert et al., 1996) is observed. Thus, the same characteristic "lower-*Re* regime" shedding-process, by means of an alternate streamwise stretching of each vortex and then the shedding of its downstream part by splitting is visualized (Fig. 4 - t^* = 7-8). However, we note that, here, the shedding initiation occurs with a slight delay as compared with the solid body (about $\Delta t^* = 1$); it will be seen that it is the opposite for the higher-*Re* regime. Besides, for the very early phase of the wake-development, another particular of the shell due to the presence of its back cavity should be mentioned. A recirculation-flow takes place even in the Stokes regime, with the two vortex cores located at the level of the cavity edges (cf. visualizations by Taneda (1979) and Abed-Meraïm

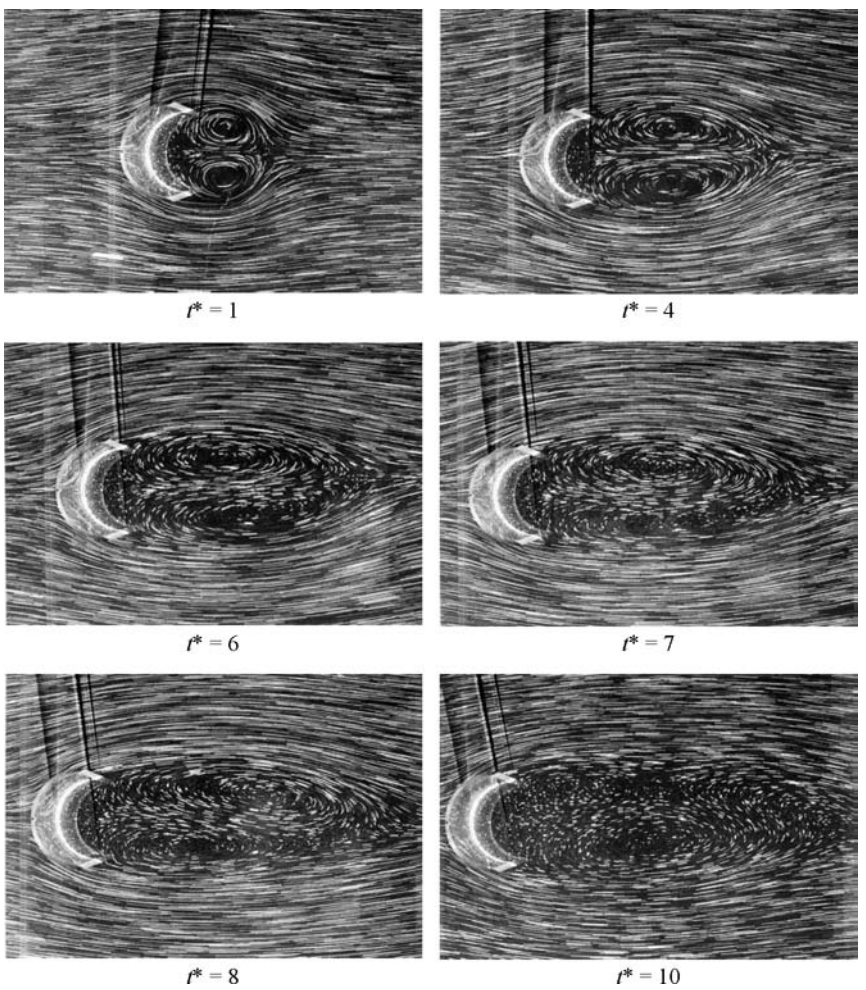

Fig. 4. Typical time-stages of the wake development behind a semicircular shell for Re = 100; mid-cross-sectional view with the incident flow from left to right.

(1992). Consequently, this configuration is also observed at the start of the motion. In fact, Figure 4 shows that the twin vortices move out of the cavity very rapidly. Already at $t^* = 1$ they have moved clearly downstream, leaving the quasi-still fluid zone in the cavity bottom.

In Figs. 5(a) to 5(e), we demonstrate the influence of an increase of the Reynolds number from 60 to 600 on the time-development of the wake-vortices of the shell for time t^* varying from 2 to 10. Thus, beyond the initial period for which the wake-vortices remain stable and attached or quasi-attached to the body edges, two regimes in the vortex-shedding process are identified, namely a lower-*Re* regime (*Re* = 60 and 100) and a higher-*Re* regime

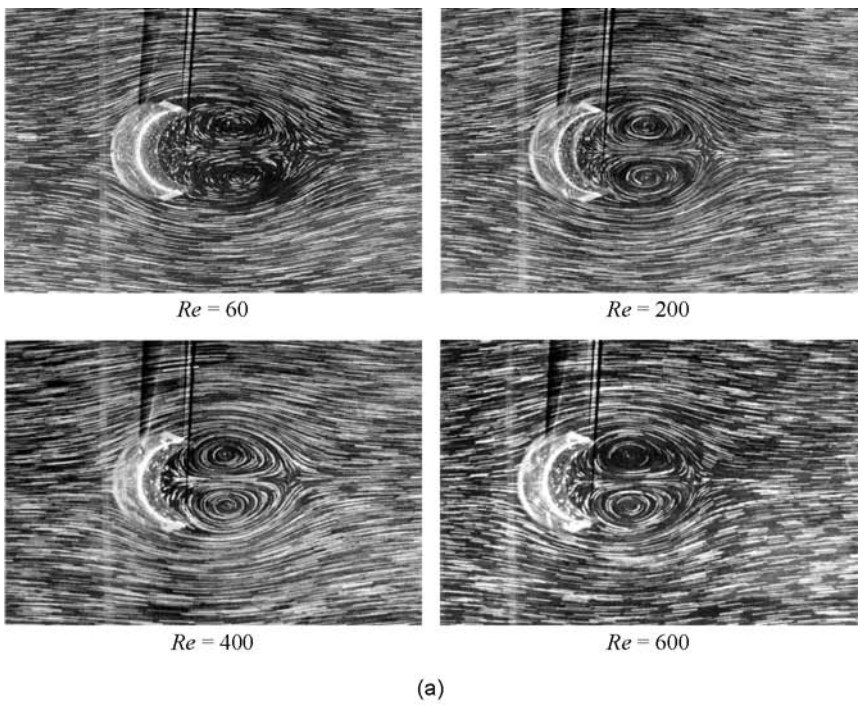

Fig. 5. Comparative flow patterns as a function of *Re* for increasing time stages; mid-cross-sectional view with the incident flow from left to right: (a) $t^* = 2$; (b) $t^* = 4$; (c) $t^* = 6$; (d) $t^* = 8$; (e): $t^* = 10$.

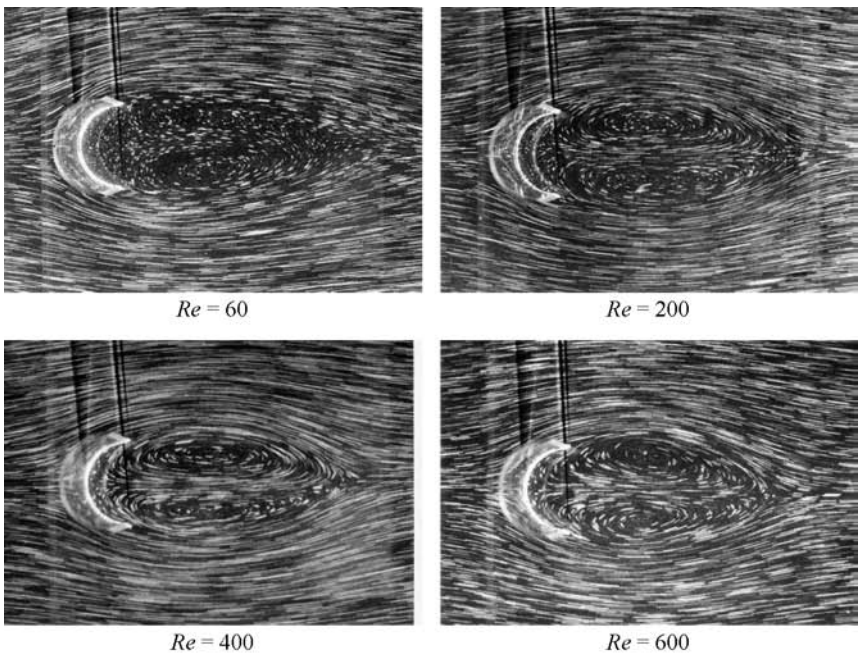

Fig. 5. (continued)

(Re = 400 and 600) with a transition Re-range around 200. The changeover appears to be associated with the occurrence of three-dimensionalities. Thus, at t^* = 2 (see Fig. 5(a)), the twin vortices appear very similar for each Reynolds number. Then an asymmetry occurs between the vortex cores at a time t^* which depends on Re, and this, not in a simple way because of the development of opposite effects. For example, as shown in Fig. 5(b), a clear and a very slight asymmetry may be detected for Re = 60 and 400 respectively but not yet for Re = 200 and 600. This asymmetry increases with time provoking the onset of the downstream shifting of one of the vortex cores and then that of the alternate vortex-shedding process itself (Figs. 5(c)-5(d)). It is mainly from this phase of the evolution that a change in the regime may be clearly detected. Thus, for the lower-Re regime (Re = 60 and 100), this shedding results from a strong stretching of alternately each of the two growing vortices, implying its splitting

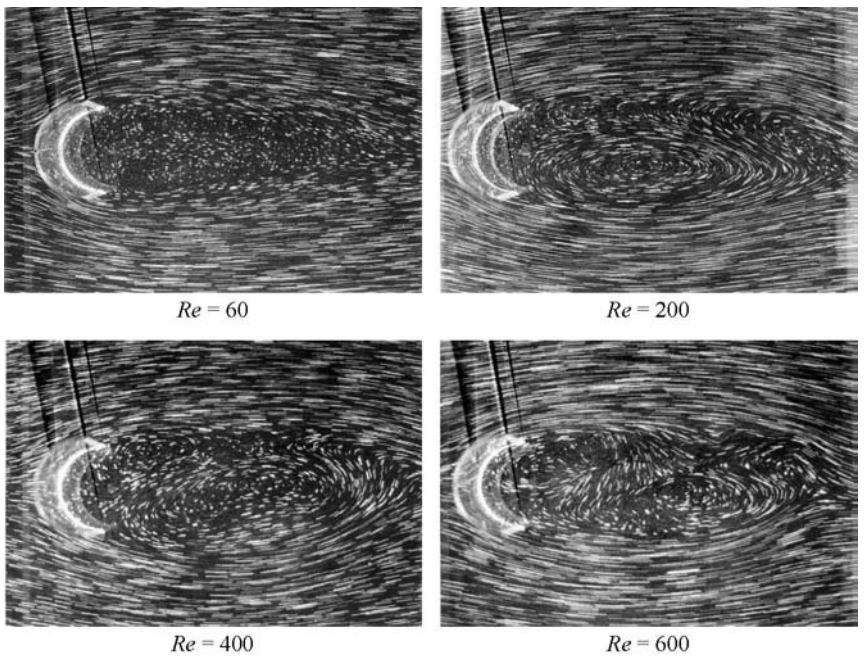

Fig. 5. (continued)

into two parts. The downstream part is effectively shed in the free stream. While the main upstream part moves back towards the body base, giving rise to a new vortex. The relative size of this retracting part decreases when *Re* increases. In fact, in the case of the shell, the maximum of the vortex elongation is observed during the shedding of the initial vortex for $Re = 100$ (see Fig. 4 - $t^* = 7$). Beyond $Re \approx 200$, the process decreases continuously with the increase of *Re*, at least up to the highest value ($Re = 600$) considered in this work. Consequently, the vortices are shed progressively in a more and more compact way implying, finally, their shedding in one piece without preliminary splitting. This shedding occurs both closer to the body base (so the near-wake extent decreases) and to the centeraxis, and after a smaller relative shifting of their cores (the primary wake instability being stronger). In the higher-*Re* regime ($Re = 400$-600) the shed-vortex cores rapidly cross the centeraxis. The change observed here in the near-wake behaviour is similar to that described by Green and Gerrard (1993) for the circular cylinder in the fully established regime. It has been shown to be linked with the evolution of the shear-stress field.

The decrease of the recirculation- or formation-zone extent for increasing *Re*, indicating that the regime has changed, is clearly pointed out by the curves of Fig. 6 giving the length L_{RZ} (for definition see Fig. 10 and the associate explanation Section 4.2) of this recirculation zone versus *Re*, for times varying between 1 and 10. L_{RZ} appears to go through a maximum for $100 < Re < 140$ when time t^* increases from 5 to 10. It should be noted that, in the second phase of the wake-development ($t^* > 5$), the rate of the variation $|\Delta L_{RZ}|/\Delta Re$ is clearly higher before reaching the maximum (i.e. for $60 < Re < 100$) than beyond (i.e. for $100 < Re < 200$). The measurement was made on each sequential photograph related to each *Re*-value; although numerous verifications have been made using several series, they do not result from averaged values. The accuracy is about 2%.

We observed that this change in regime is associated with the occurrence of different types of three-dimensionalities. One of these 3D-manifestations is pointed out by the evolution of the cross-sectional shape of the vortex cores which turn into foci. It will be seen, in the following section, that this phenomenon is caused by the occurrence of two opposed spanwise currents, which arise from each endplate, and penetrate progressively the B-K vortex tubes. Such foci are first discernible at $Re = 200$. They are promoted by the increase of *Re*, and occur earlier : $t^* \approx 7$ for $Re = 200$, $t^* \approx 5$ for 600 i.e. respectively after and before the vortex-shedding initiation. The presence of spanwise currents appears to delay clearly this shedding initiation and even the onset of the vortex-core asymmetry itself. However, once initiated, the B-K shedding process is again accelerated by the increase of *Re* i.e. the increase of inertia. Thus, at the final time of observation $t^* = 10$, two vortices have been shed for $Re = 600$ (Fig. 5(e)) or in the process of being shed, like for $Re = 200$ and 400. But these vortices are strongly three-dimensional and are destroyed by very first manifestations of turbulence.

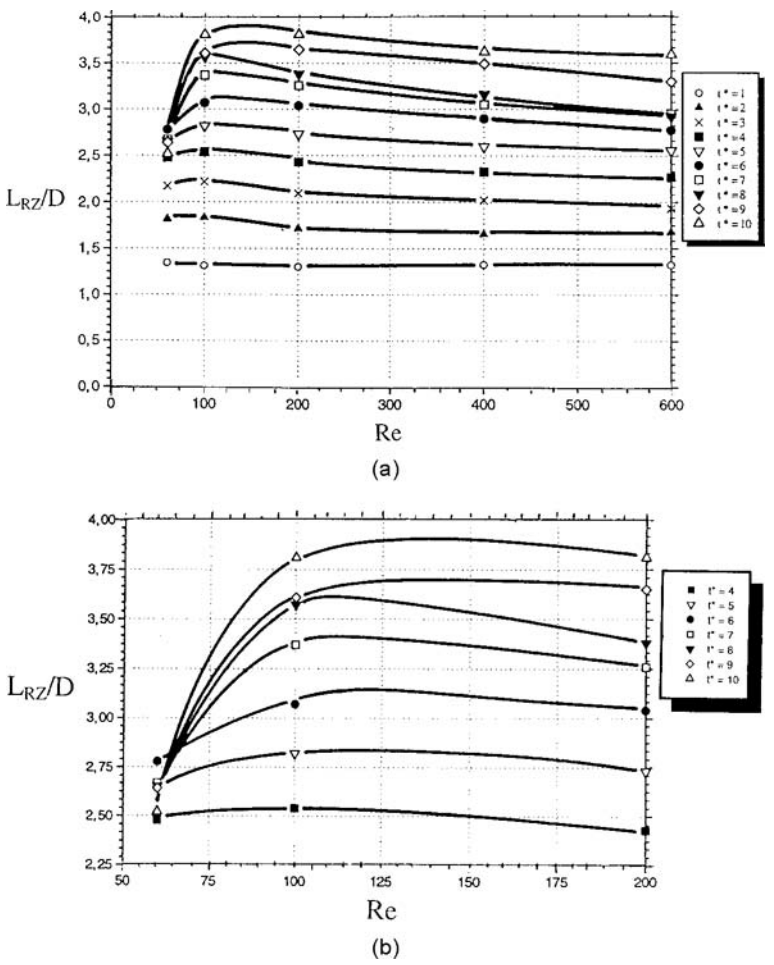

Fig. 6. The normalized recirculating-zone length L_{RZ}/D as functions of Re and t^* ($1 \le t^* \le 10$): (a) general evolution for $60 \le Re \le 600$; (b) detail for $60 \le Re \le 200$ (for the L_{RZ} definition, see Fig. 10).

On another hand, for $Re \ge 200$, we will show that intrinsic three-dimensionalities also occur and give rise to well formed spanwise structures which contribute to decrease the 3D-endplate interaction.

4. Wake-flow Structure in the Mid-span Plane

4.1 Visualization of Typical Spanwise Currents

The existence of spanwise currents coming from the endplates and the way they propagate with time into the core of each of the two B-K vortex tubes is shown in Fig. 7 by means of the rolling up of the tin salt filaments. The central parts appear to progress spanwise helically into typical cones, like in the circular cylinder case (Pineau, 1992; Pineau et al., 1992). This white "dye" is emitted continuously from the electrolysis of 3 tin wires (Fig. 8(a)) which are rolled up around 3 cross-sections of the shell located respectively at a distance of $0.5D$ (wire 1), $1.5D$ (wire 2), $2.5D$ (wire 3) from the endplate. So only one half of the span was equipped. Until the onset of the twin vortex asymmetry, the two conical tips of the filaments, penetrating the two B-K-vortex tubes, are superposed on the proposed view and appear as unique. Subsequently, the relative shifting of the cores implies that of the dye cones; a first shifting is well discernible from $t^* = 5$, especially on filaments n° 2 and 3 (Fig. 7). An evaluation of the time-progression of the cone tips in the span direction is given by the curves of Fig. 8(b). They exhibit a quasi-linear part. Along this linear part the speed of progression is about $0.30V_0$. Later on, they are slown down by the presence of the opposite currents coming from the other half part of the shell. At $t^* = 7$, the dye filament become blurred by turbulent diffusion. For the same reason, as indicated in sec. 3, this type of visualization has been carried out only for $Re = 600$.

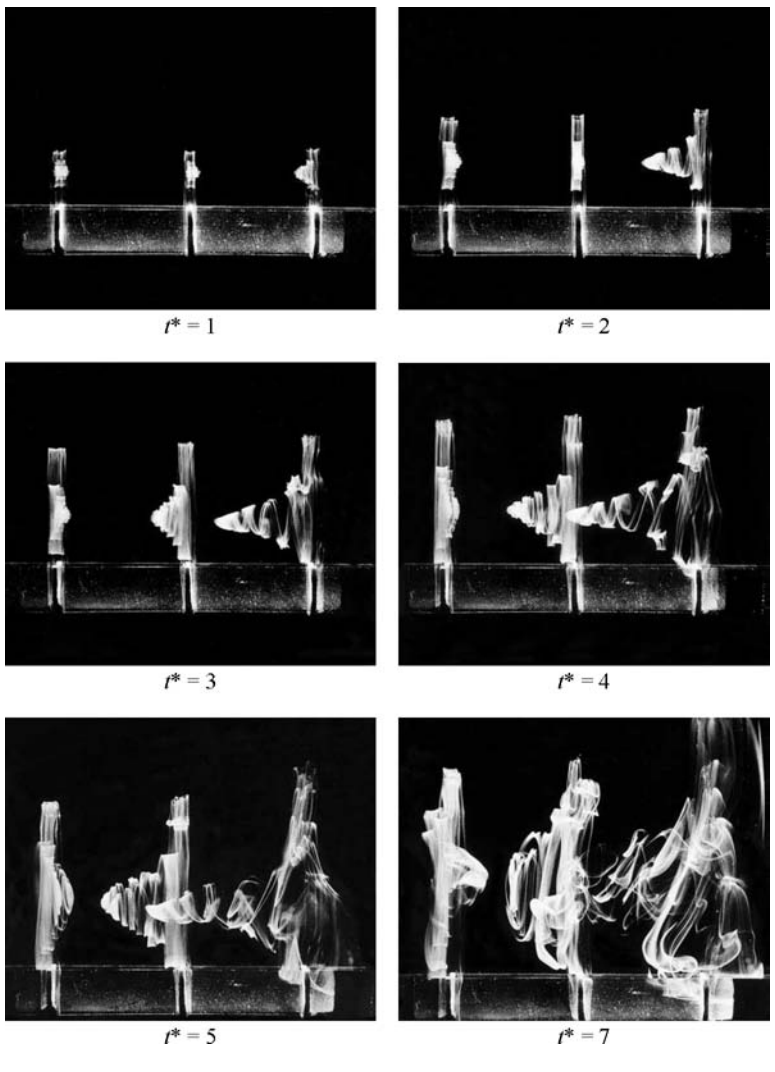

Fig. 7. Visualization, on half the shell span, of the birth and progression of spanwise currents originating from the endplate; the mid-cross section of the shell is at the level of the first white ring on the left, the endplate is at the right edge of the picture; the incident flow runs upwards; *Re* = 600.

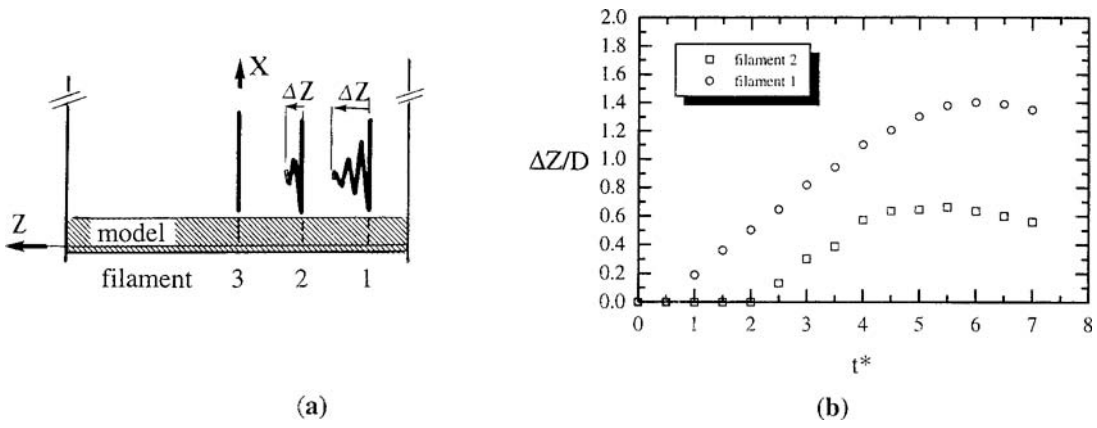

Fig. 8. Time spanwise-progression of the tip of the electrochemical filaments n°1 and n°2: (a) explanatory schematic; (b) corresponding curves.

4.2 Spanwise Particle-streak Visualization

The particle-streak method has also been used to show the spanwise time-evolution of the flow topology for the full studied *Re*-range. Thus, now the sheet of light illuminates the mid-span plane.

As a particularly interesting case, we have collected in Fig. 9 the sequential pictures related to *Re* = 400 showing the wake development in this mid-span plane when t^* varies from 2 to 10. The flow again runs upwards, the upstream generating line of the shell, seen now in full length, appears as a white horizontal line at the bottom of each picture. Because of its transparency, it is also possible to identify the trace of the forward sharp edge of the shell, a tenth of the body length above. It is recalled that the body is limited spanwise by two endplates (according to Fig. 2(a)). The vertical traces of these endplates can be seen on each side of the picture. In fact, only the lower parts are visible. The upper parts, which extend beyond the upper edge of the photo are hidden by the forward towing rods (Fig. 2(a)). These rods do not perturb the flow because they are not in the lit plane. As a guide, the different types of structures susceptible to appear in the mid-span-plane are identified in the schematic of Fig. 10 (BB-section). Thus, in the spanwise view, the flow may be divided into 3 zones. Zone I, below the model, is the

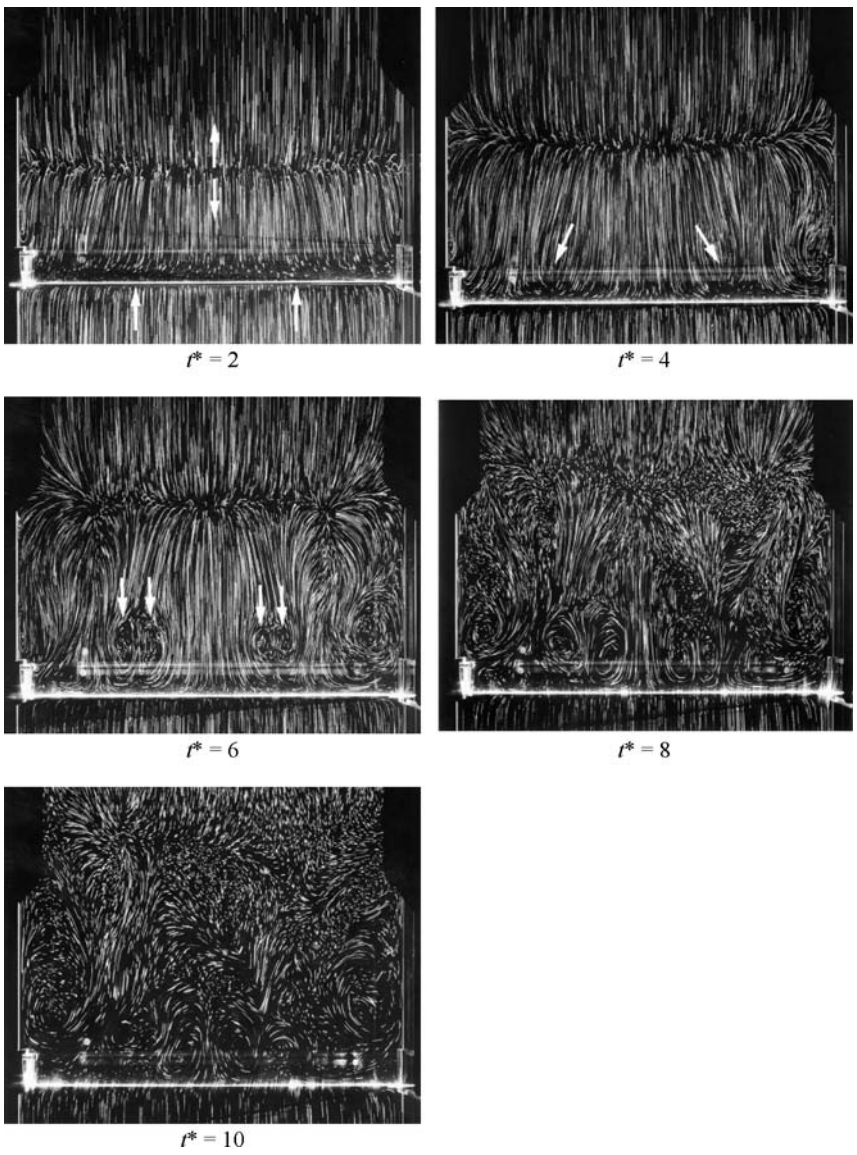

Fig. 9. Time-sequence of the flow pattern visualized in the mid-span plane of a semicircular shell; the incident flow is running upwards, *Re* = 400 (see also explanatory schematics of Fig. 10). It should be noted that the upper parts of each of the vertical endplates traces are hidden by forward towing rods.

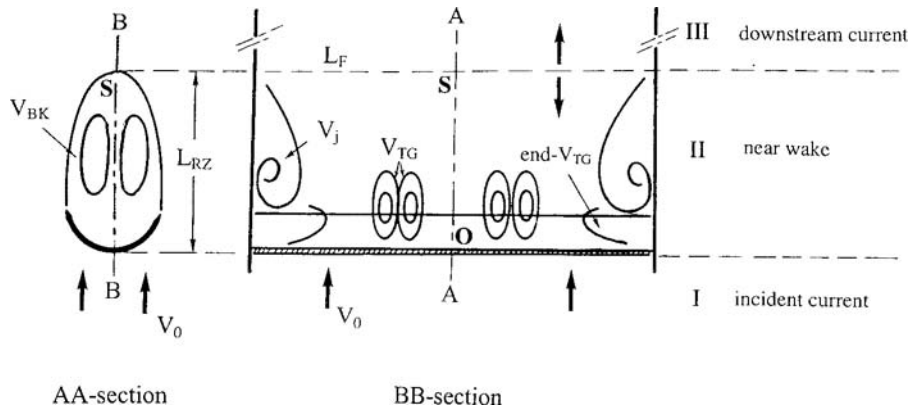

Fig. 10. Explanatory schematics of the different vortical structures encountered in the mid-span-sectional view of the semicircular shell wake.

incident current. Zone Ⅱ, is the recirculating near wake; it is limited by line L_F where either the fluid velocity is zero or perpendicular to the plane under consideration. Thus, the frontier L_F separates the near wake from the general downstream current. The flow within zone Ⅱ runs downwards i.e. towards the body base. It is in this part that the B-K-vortices (V_{BK}) form and develop as shown in the associated cross-section AA of Fig. 10. Other vortices have also been schematized, such as the so-called corner or junction vortices V_j and the typical Taylor-Görtler-like V_{TG} secondary vortices which emerge for $Re > Re_t$ ($Re_t \approx 200$) with increasing time. The V_j-vortices are induced by the endplates, whereas the V_{TG}-vortices are due to an intrinsic secondary instability of the wake flow. Finally in zone Ⅲ, the flow is again oriented upwards.

The emergence and time-development of these different types of vortical structures can be followed in Fig. 9 for $Re = 400$.

At the first stage $t^* = 2$, the particle-streaks of zone Ⅱ are roughly parallel and aligned with the free stream in the main part of the span, pointing out the quasi 2D-character of the wake with a quasi-horizontal frontier-line L_F limiting the recirculating flow. However, at each spanwise extremity of this zone Ⅱ, a thin junction vortex V_j is already forming along each endplate. They are induced by the necessary matching of the main current passing around the shell with the developing endplate boundary layer; so they are effectively induced by end-effects.

At $t^* = 4$, the V_j-vortices have clearly increased in size and in strength, whereas line L_F becomes distorted at its extremities under the local occurrence of 3D source-like flows. Furthermore, just right behind the shell, incipient vortices may be detected, on each side of the central part of the span. They are indicated by the white arrows.

At $t^* = 6$, these new vortices are structured into two pairs of contrarotary vortices of Taylor-Görtler type (V_{TG}). In the next section, we will show that they could be effectively induced by the increase of the centrifugal forces of the rotating B-K-vortex flow whose development is promoted by the concave shape of the shell wall. At the level of the endplates, two superposed vortices coexist. The upper one is the increased initial V_j-vortex which has moved downstream, pushed by the occurrence of an end V_{TG}-vortex.

At $t^* = 8$, a V_{TG}-vortex pattern is clearly formed. The frontier-line L_F of the recirculation zone, still globally horizontal, becomes rather blurred under the combined influences of the onset of the B-K vortex-shedding process (see Fig. 5(d)) and the increasing action of different types of 3D-disturbances. A moment later, i.e. $t^* = 10$, the whole flow structure of zone Ⅱ appears blurred.

The way this time-evolution is influenced by the Reynolds number is shown in Figs. 11(a) to 11(e). At $t^* = 2$, the flow structure appears similar for all Re, as it was the case in the cross-section (Fig. 5(a)). But, again differences clearly appear for $t^* \geq 4$ (Figs. 11(b) to 11(e)). On one hand, the V_j-junction-vortices are bigger when Re is lower. Whereas, on the contrary, the V_{TG} vortices are promoted in strength and number by the increase of Re. Thus, for $Re = 60$ no V_{TG}-vortices arise until $t^* = 10$. Their very first manifestation is discernible only at $Re = 200$. However, their formation is clearer when Re is increased and time has elapsed ($t^* > 4$), at least until they become destroyed by turbulence. This destruction occurs more rapidly (Figs. 11(d)-11(e)) as Re increases ($t^* = 8, 10, > 10$ for $Re = 600, 400, 200$ respectively). The wavelength of these V_{TG}-structures appears to change abruptly above $Re = 200$ since, for the optimal time $t^* = 8$, only the primers of a pair of vortices are clearly formed at $Re = 200$, whereas two pairs plus two end V_{TG}-vortices take place for $Re = 400$ and 600.

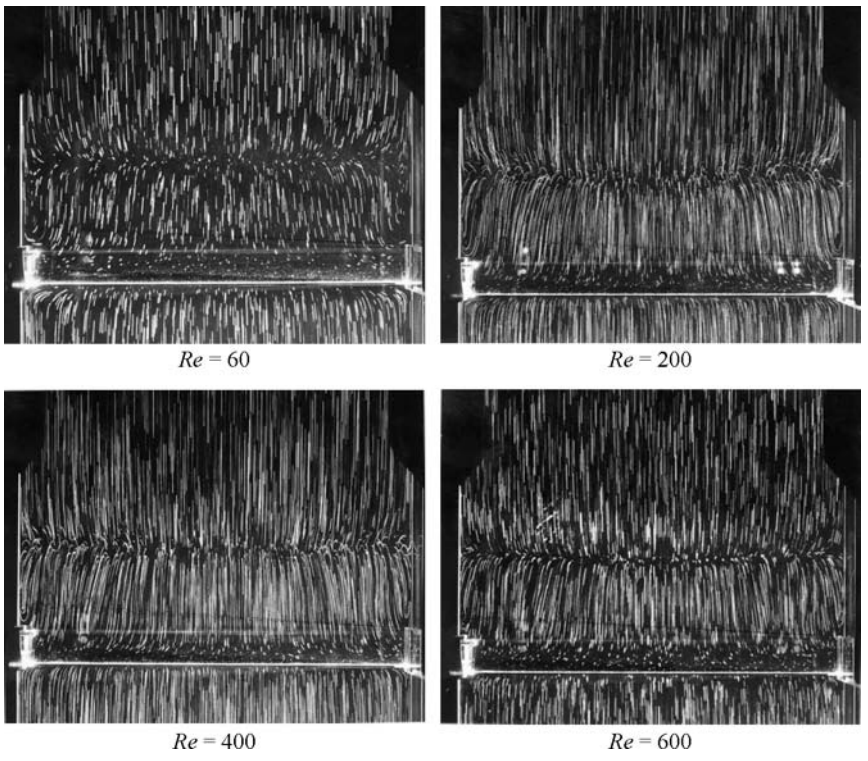

Fig. 11. Comparative spanwise flow patterns as a function of *Re*, for increasing time-stages; mid-span-sectional view with the incident flow upwards: (a) $t^* = 2$; (b) $t^* = 4$; (c) $t^* = 6$; (d) $t^* = 8$; (e) $t^* = 10$.

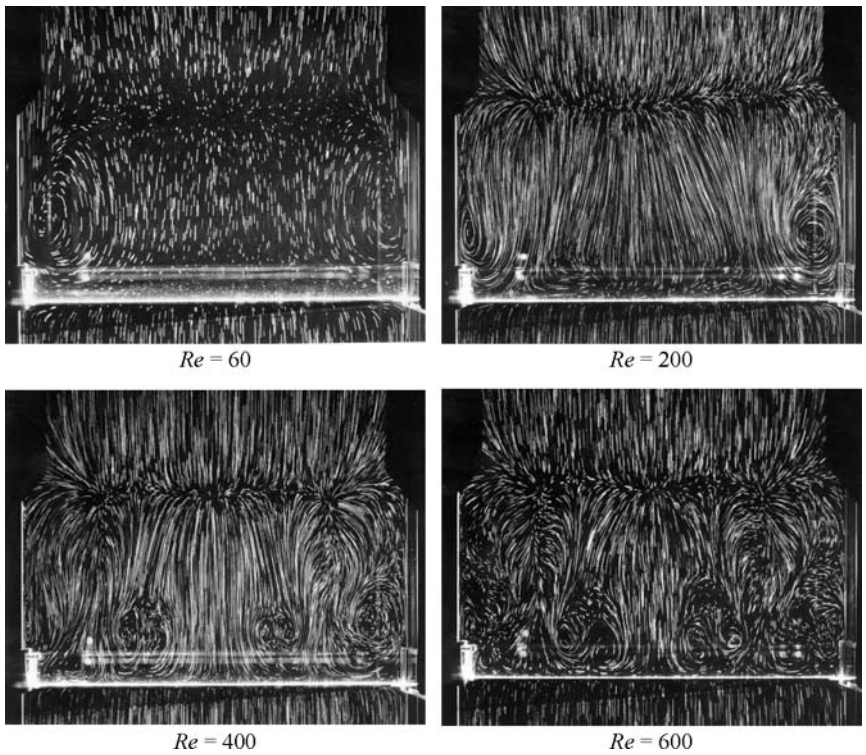

(c)

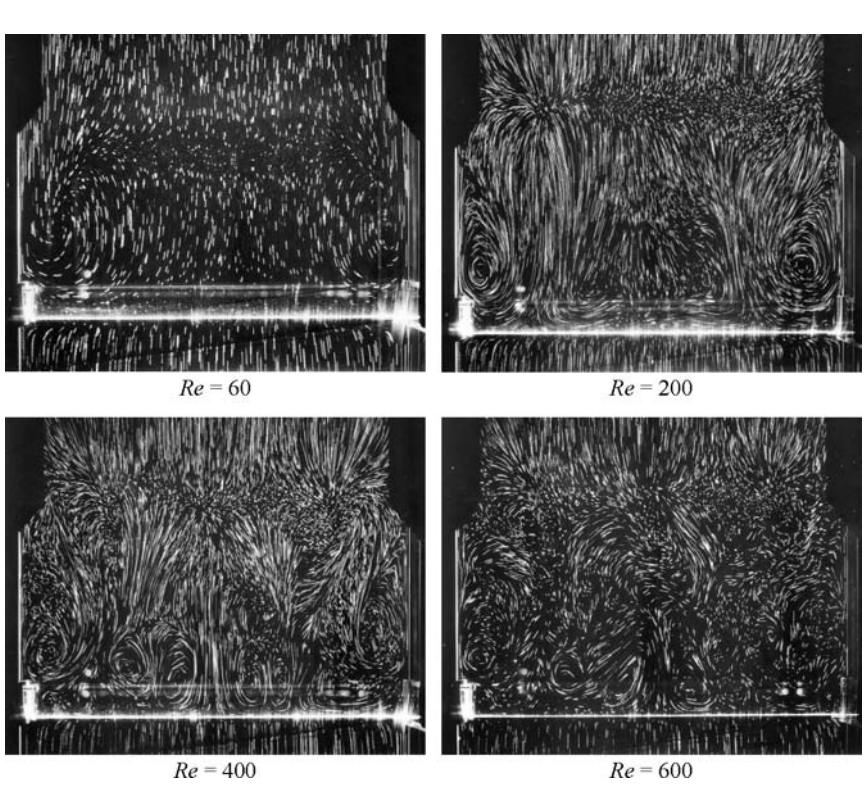

(d)

Fig. 11. (continued)

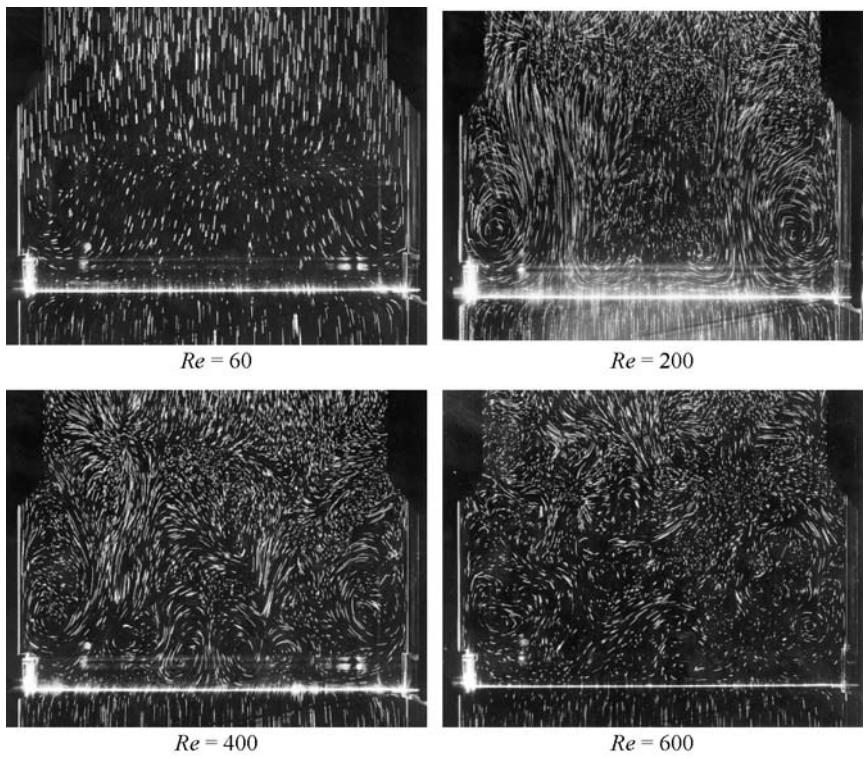

Fig. 11. (continued)

5. A Preliminary Approach of the Secondary Wake-instability

According to the proposition of Coutanceau and Defaye (1991) and Zhang et al. (1994) and also to parallel experiments conducted in lid-driven cavities (Migeon et al., 1995; Coutanceau et al., 1996), it is thought that the patterns of TG-vortices could be the manifestation of centrifugal instabilities taking place in the rotating fluid-layers of the Bénard-Kàrmàn vortices. To give a preliminary estimation of the degree of instability of these rotating layers, we have determined the radial upstream and downstream velocity profiles $V(r)$, along the mid-horizontal $\boldsymbol{r}_1$- and $\boldsymbol{r}_2$-axis passing through the forming vortex (see Fig. 12(b)). In fact, in relation with the inviscid Rayleigh stability criterion ($\boldsymbol{\Phi} \geq 0$ where $\boldsymbol{\Phi}$ is the Rayleigh discreminate $\frac{1}{r^3}\cdot\frac{d}{dr}(rV)^2$), we have considered the evolution of the quantity $(rV)^2$ along the above mentioned radial-axes in function of the Reynolds number, at the selected time $t^* = 6$ (see Figs. 12(a) to 12(c)). These profiles exhibit a potentially unstable part ($d(rV)^2/dr < 0$), upstream of the velocity maximum for all Re. However, because of the damping effect of viscosity, the instability develops only when the slope of the curve becomes sufficiently high, namely for $Re \geq 200$. Likewise, although the TG-vortices take their origin in the shell bottom, under the viscosity effect, they develop largely outside the upstream part of the profile. They contaminate progressively the whole upstream rotating layer, i.e. up to the B-K vortex center itself (see Fig. 1).

It is obvious that the present consideration constitutes only a very rough approach of the problem since the square kinetic momentum has been estimated in the mid-cross section whereas the TG-vortices develop on each side of this cross section. A more complete investigation is necessary for a clearer insight, taking into account viscosity effects, unsteady effects induced by the flow acceleration, as well as the three-dimensional aspect of the wake structure.

6. Conclusion

The present work provides new flow-visualization data on 3bluff-body wake formation in the Re-range $60 \leq Re \leq 600$ including transition regime. These data are related to both the primary and secondary wake instabilities which

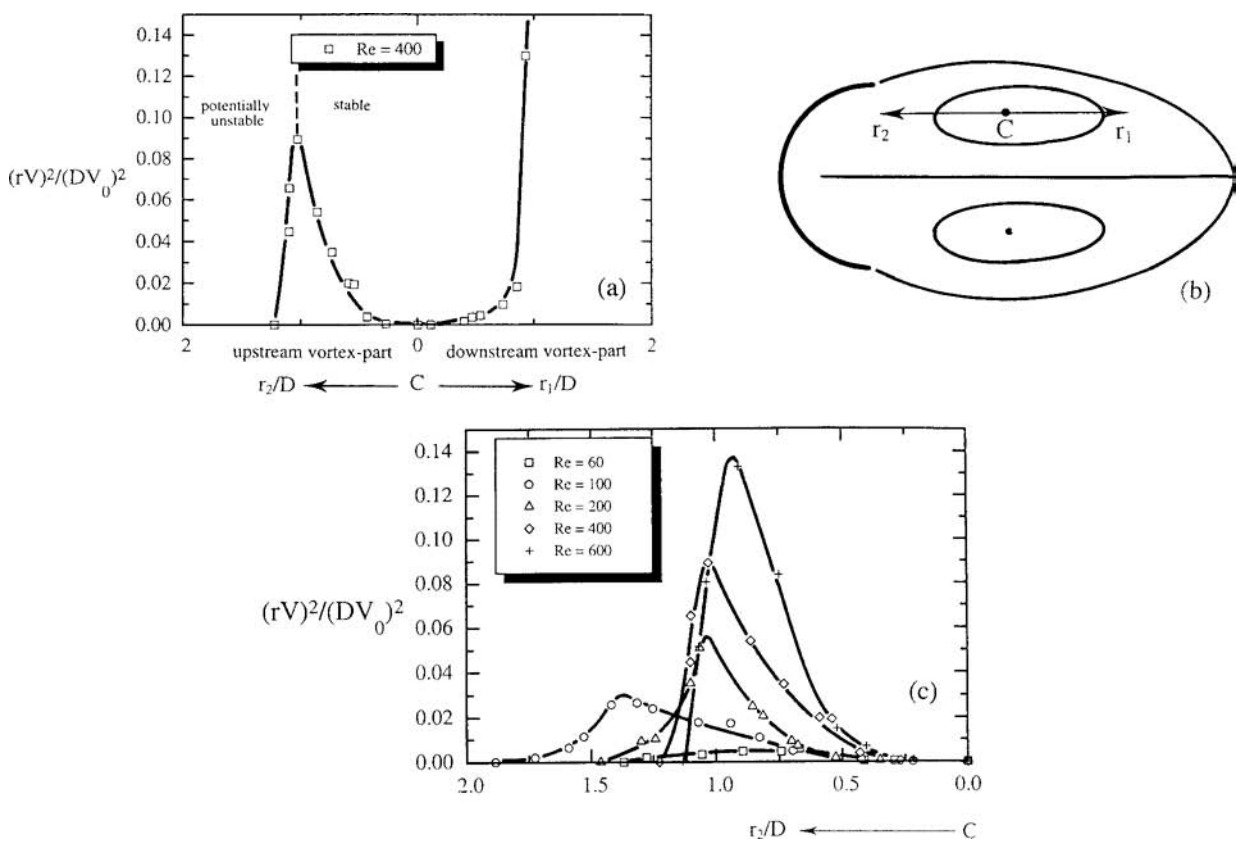

Fig. 12. Evolution along the horizontal radial vortex axes of the quantity $(rV)^2$ as function of the Reynolds number: (a) a complete typical profile for Re = 400; (b) explanatory schematic identifying the considered axes r_1 and r_2; (c) comparison in function of Re of the upstream part of the profiles.

settle with time and with the increase of Reynolds number, respectively. They are valid for the mid-cross and mid-span section of a semicircular shell with an aspect ratio of 5.2, after an impulsive start in uniform translation.

On one hand, it is established that the presence of the back hollow face of the shell does not modify significantly the process of formation of the Bénard-Kàrmàn vortices, compared with the similar solid body (previously considered by Boisaubert et al., 1996), showing the same type of changover in the shedding mode from Re between 100 and 200. In the lower-Re regime ($Re \approx$ 60-100), the shedding takes place under a strong preliminary stretching of the vortices and then their splitting into two parts, whereas in the higher-Re regime (Re = 400-600), the vortices detach in one piece inducing a shortening of the formation zone. The corresponding change in the time-evolution of the formation-length in function of Reynolds number has been found to take place at a slightly lower value than in the solid case (Re_c between 120-140 instead of 190). For Re = 600, similar Kelvin-Helmholtz instabilities have also been detected in the separated shear layers originating from the sharp body edges. However, the shell wake is characterized by a Stokes recirculation. Consequently, this recirculation arises as soon as the motion is started. For equivalent values of the parameters (t^*, Re), the length of the recirculating fluid is about a shell depth longer. This fact may be used to favour mixing processes in applications.

On the other hand, the complementary investigation in the mid-span plane shows that the back concave wall of the shell plays an important role in the progressive temporal development of the induced and intrinsic three-dimensionalities which superpose on the primary wake vortices. In fact, the selected body shape permits to differentiate clearly these three-dimensionalities and to deduce the consequence of their emergence on the global near-wake structure.

Thus, we have been able to distinguish :

(i) end-vortices and spanwise currents induced by the end-plates limitating the shell span. It has been shown that the spanwise currents, which penetrate the B-K vortex tubes, should act as rather rigid skeletons and delay

the initiation of the primary wake instability.
(ii) Taylor-Görtler-like vortices provoked by the secondary instability of the wake flow. The first emergence of these T-G vortices was found for Re = 200 and from t^* = 4 onwards as primers of a vortex pair. Whereas for Re = 400 and 600, clear patterns of two pairs of T-G vortices plus two end T-G vortices have been visualized. Unfortunately, such T-G patterns are only observable during a short period of time because they become rapidly blurred under the onset of turbulence, and this, the sooner the higher Re is (t^* = 8, 10, > 10 for Re = 600, 400 and 200, respectively). Although, these V_{TG}-vortices imply the wake flow to be clearly 3D in details, they maintain it in a global 2D-configuration with a roughly straight frontier line parallel to the body generatrix, as opposed to what happens with the equivalent solid semicircular cylinder, similarly limited in span by the same endplates. Indeed, for this solid body, the end effects appeared to be dominant and to prevent the clear emergence of TG-vortex pattern, inducing a highly three-dimensional final near-wake flow in the same Re-domain of investigation. It was found that it is also the case for any of the other typical solid body-shapes studied by Coutanceau et al. (1998). The perpendicular flat-plate wake appears to be the most affected one by this global 3D-distortion (Coutanceau and Ehrmann, 1998).

The role of the endplate effects in preventing the V_{TG}-pattern emergence was confirmed by Bigeault (1998) using the same experimental set up as ours. Indeed, a well formed V_{TG}-pattern clearly reappears when these effects are suppressed by an adequate inclination of the endplates. Under these conditions, the frontier of the recirculating-zone takes again a quasi-2D character.

This proves that the aspect of the final spanwise wake structure of short cylindrical bodies, limited by endplates, results from the competition between induced end-vortices and intrinsic TG-vortices. For the selected aspect ratio of 5.2, this competition is clearly in favour of the intrinsic vortices in the case of the hollow back-face shell as opposed to what happens with similar solid bodies. However, these intrinsic TG-vortices can also be dominant for such solid bodies by erasing the end effects.

Further experimental and numerical studies should be conducted to bring complementary data in this fundamental problem. Presently, a parallel experimental investigation, related to the flow establishment inside lid-driven cavities of different cross-sectional shapes, including the semicircular one, is carried out using the same visualization principle. Clear Taylor-Görtler patterns have again been found to develop in the unstable part of the rotating layer of the primary vortex by Migeon et al. (1995), Coutanceau et al. (1996) and Migeon (2000) for each cross-sectional shape, confirming our shell-wake interpretation.

Acknowledgements

The authors are very much indebted to the referees for their very valuable comments and relevant suggestions.

References

Abed-Meraïm, K. and Coutanceau, M., Etude de l'écoulement plan engendré par la translation d'une cavité semi-circulaire par visualisation particulaire, In Visualisation et Traitement d'Images en Mécanique des Fluides, (Ed. M. Stanislas and J.C. Monnier, (1990),278-284., Institut de Mécanique des Fluides de Lille.

Abed-Meraïm, K., Etude expérimentale de l'écoulement plan engendré parla translation d'une coque semi-circulaire pour des nombres de Reynolds allant de 0 à 40, Thèse de l'Université de Poitiers, France (1992).

Albarède, P. and Provansal, M., Quasi-periodic cylinder wakes and the Ginzburg-Landau model, J. Fluid Mech., 291 (1995), 191-222.

Barkley, D. and Henderson, R. D., Three-dimensional Floquet stability analysis of the wake of a circular cylinder, J. Fluid Mech., 322 (1996), 215-241.

Bigeault, K., Etude expérimentale de l'influence de l'inclinaison des plaques de maintien d'un cylindre semi-circulaire sur le développement de son sillage, D. E. A. Université de Poitiers (1998).

Boisaubert, N., Coutanceau, M. and Ehrmann, P., Comparative early development of wake vortices behind a short semicircular-section cylinder in two opposite arrangements, J. Fluid Mech., 327 (1996), 73-99.

Chyu, C. and Rockwell, D., Evolution of patterns of streamwise vorticity in the turbulent near wake of a circular cylinder, J. Fluid Mech., 320 (1996), 117-137.

Coutanceau, M. and Defaye, J. R., Circular cylinder wake configurations: a flow visualization survey, Appl. Mech. Rev., 44 (1991), 255-305.

Coutanceau, M. and Ehrmann, P., Setting up of three-dimensional endplate effect on the starting wake of a perpendicular flat plate, J. of Visualization, 1, 1 (1998), 4.

Coutanceau, M. and Pineau, G., Some typical mechanisms in the early phase of the vortex-shedding process from particle-streak visualization, Atlas of Visualization Ⅲ, Ed. The Visualization Society of Japan, (1997), 43-68, CRC Press.

Coutanceau, M., Ehrmann, P. and Boisaubert, N., Some new insights on the onset and development of three-dimensional end effects and secondary instability in the wake of quasi-2D obstacles, CD ROM Proceedings of the 8th International Symposium on Flow Visualization, Ed. G. M. Carlomagno and I. Grant, (1998).

Coutanceau, M., Migeon, C., Pineau, G. and Texier, A., Starting flow inside a rectangular-section cavity as function of Reynolds number, Proceedings of the fourth Asian Symposium on Visualization, Ed. Q.D. Wei, (1996),65-68, International Academic Publishers.

Ehrmann, P., Etude comparative de la formation des sillages en fonction de la forme des obstacles, Application à la coque semi-circulaire, Thèse

de l'Université de Poitiers, France (1996).
Green, R. B. and Gerrard, J. H., Vorticity measurements in the near wake of a circular cylinder at low Reynolds numbers, J. Fluid Mech., 246 (1993), 675-691.
Hasimoto, H., Creeping viscous flow past a circular arc with special reference to separation, J. Phys. Soc. Japan, 47 (1979), 347-348.
Karniadakis, G. E. and Triantafyllou, G. S., Three-dimensional dynamics and transition to turbulence in the wake of bluff bodies, J. Fluid Mech., 238 (1992), 1-30.
Leweke, T. and Provansal, M., The flow behind rings: bluff body wakes without end effects, J. Fluid Mech., 288 (1995), 265-310.
Mansy, H., Yang, P. M. and Williams, D. R., Quantitative measurements of three-dimensional structures in the wake of a circular cylinder, J. Fluid Mech., 270 (1994), 277-296.
Massons, J., Gavalda, Jna., Ruiz, X. and Diaz, F., Image analysis of the wake generated by a Savonius rotor, Wind Eng., 12, 6 (1988), 341-351.
Migeon, C., Etude comparative de la structure des écoulements primaire et secondaires s'établissant dans différents types de cavités cylindriques, Thèse de l'Université de Poitiers, France, (to appear 2000).
Migeon, C., Pineau, G., Coutanceau, M. and Gad el Hak, M., Early time-development of lid-driven cavity flows, Flow Visualization Ⅶ, Ed. J. Crowder.(1995), 54-58 Begell House, Inc.
Noack, B. R. and Eckelmann, H., A global stability analysis of the steady and periodic cylinder wake, J. Fluid Mech., 270 (1994), 297-330.
Noack, B. R., König, M. and Eckelmann, H., Three-dimensional stability analysis of the periodic flow around a circular cylinder, Phys Fluids A5 (1993), 1279-1281.
Pineau, G., Mise en évidence et évaluation des effets tridimensionnels dans l'écoulement instationnaire autour d'un cylindre circulaire d'envergure finie, Thèse de l'Université de Poitiers, France (1992).
Pineau, G., Texier, A., Coutanceau, M. and Ta Phuoc Loc, Experimental and numerical visualization of the 3D-flow around a short circular cylinder fitted with end-plates, In Flow Visualization Ⅵ, Ed. Y. Tanida and H. Miyashiro, (1992), 343-347, Springer Verlag.
Polidori, G., Etude par visualisation de sillages tridimensionnels, Application à un profil d'aile rectangulaire, Thèse de l'Université de Poitiers, France (1994).
Polidori, G., Pineau, G., Abed Meraïm, K. and Coutanceau, M., Shedding Process of the Initial Vortices from Impulsively Started Cylinders at Re = 1000; End and Body Geometry Effects, In Bluff-Body wakes, Dynamics and Instabilities, Ed. H. Eckelmann, J.M.R. Graham, P. Huerre and P.A. Monkewitz, (1992), 285-288, Springer Verlag.
Prasad, A. and Williamson, C. H. K., The instability of the shear layer separating from a bluff body, J. Fluid Mech., 333 (1997), 375-402.
Rosko, A., On the development of turbulent wakes from vortex streets, NACA Rep., 1191 (1954), 1-25.
Taneda, S., Visualization of separating Stokes flows, J. Phys. Soc. Japan, 46 (1979), 1935-1942.
Tomboulides, A. G., Triantafyllou, G. S. and Karniadakis, G. E., A new mechanism of period doubling in free shear flows, Phys. Fluids A4 (1992), 1329-1332.
Tritton, D. J., Experiments on the flow past a circular cylinder at low Reynolds numbers, J. Fluid Mech., 6 (1959), 547-567.
Williamson, C. H. K., Three-dimensional wake transition, J. Fluid Mech., 328 (1996a), 345-407.
Williamson, C. H. K. Vortex dynamics in the cylinder wake, Ann. Rev. Fluid Mech., 28 (1996b), 477-539.
Wu, J., Sheridan, J., Welsch, M. C. and Hourigan, K., Three-dimensional vortex structures in a cylinder wake, J. Fluid Mech., 312 (1996), 201-222.
Zhang, H. Q., Fey, U., Noack, B. R., König, M. and Eckelmann, H., On the transition of the cylinder wake, Phys. Fluids, 7 (4) (1995), 779-794.
Zhang, H. Q., Noack, B. R. and Eckelmann, H., Numerical computation of the 3-D cylinder wake, Report No 3/1994, Max-Planck-Institut für Strömungsforschung, Göttingen (1994).

Author Profile

Madeleine Coutanceau: She was (up to 1995) Professor of Fluid Mechanics at the University of Poitiers, France, from which she received her Doctorat ès Sciences in 1971. She was at the head of a research group working mainly in the domain of flow visualization. Her main themes of research include the investigation of viscous flows around obstacles with rigid or free surfaces, such as drops and bubbles, in Newtonian and non-Newtonian liquids, and the time development of wakes around bluff bodies and aerodynamic profiles subjected to various motions after an impulsive start. She is currently an Honorary Professor of the University of Poitiers, a member of the Association Universitaire de Mécanique, of the Scientific Committee of the Colloque National de Visualisation et de Traitement d'Images en Mécanique des Fluides and of the International Organizing Board of the International Symposium on Flow Visualization.

Christophe Migeon: He received his master degree from the University of Poitiers, France, in 1995. He is currently about to get his Ph.D. in Aerodynamics and Fluid Mechanics from the same University. His theme of research is related to the two- and three-dimensional study of various lid-driven cavity-flows. At the same time, he is a lecturer at the Institut National de Sciences Appliquées (INSA) in Rennes, France.

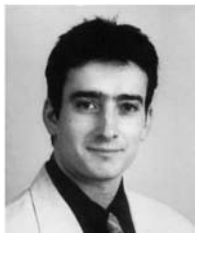

Patrick Erhmann: He received his master degree (1992) and his Ph.D. (1996) from the University of Poitiers, France, in the domain of Aerodynamics and Fluid Mechanics. His theme of research was related to the comparative study of wake formation as function of the body shape. He is currently a manager in the french automotive branch of a US firm.